Analytic description of the magnetization-reversal phase diagram in thin films with uniaxial perpendicular magnetic anisotropy

Sug-Bong Choe and Sung-Chul Shin
Department of Physics and Center for Nanospinics of Spintronic Materials, Korea Advanced Institute of Science and Technology, Daejeon 305-701, Korea
(Received 9 September 2003; revised manuscript received 2 March 2004; published 13 July 2004)

We present an analytic description of magnetization-reversal phases based on a micromagnetic theory. Calculated phase diagrams characterize three contrasting domain evolution patterns: wall-motion, dendritic-growth, and nucleation dominant phases. Gradual phase transitions are observed with respect to the magnetostatic energy, the domain-wall energy, and the temperature, while minor phase shifts are seen with respect to the anisotropy, the cell volume, the applied field, and the simulation size. Variation in the local anisotropy of only a few percent induces phase transitions.

DOI: 10.1103/PhysRevB.70.014412 PACS number(s): 75.60.Jk, 75.70.Kw, 75.50.Ss

I. INTRODUCTION

During the last few decades magnetization-reversal dynamics in uniaxial ferromagnetic thin films has become a challenging issue in magnetism. The interest in studying these dynamics is due to the intense interest in magnetic information technology, in which the reversal process of magnetic domains is inherently involved.[1–3] Direct domain observations by means of advanced magnetic imaging technologies[4,5] have shown that magnetization reversal takes place via three fundamental domain evolution processes: nucleation, dendrite-growth, and wall motion. Contrasting reversal behaviors come from the counterbalance of these processes. Much effort has been devoted to clarifying their origins. Structural imperfections, such as interfacial roughness, lattice mismatches, local structural variation, or local magnetic variation, have been suggested as possible origins.[6–11] On the other hand, macroscopic magnetic properties depending on either film composition or layer structure, have been examined as another origin of the phenomena.[12–16]

Theoretical micromagnetic calculations predict that magnetization-reversal dynamics are sensitive to either the macroscopic magnetic properties[17–20] or the local structural imperfections.[9,10,21,22] A micromagnetic algorithm of magnetization reversal in thin films with perpendicular magnetic anisotropy was proposed by Mansuripur[23] two decades ago to exploit the writing mechanism of magneto-optical recording media. The contrasting domain patterns between the wall motion and the nucleation dominant reversal were first demonstrated by Kirby *et al.*[17] among uniform films having a different domain-wall energy. Lyberatos *et al.*[18,19] developed a more generalized micromagnetic algorithm for various physical situations, including the dendritic-growth reversal phase. Several other models have been presented to explain the magnetization-reversal behaviors in different systems.[15,20] On the other hand, the contrasting change in magnetization-reversal behavior was also explained by introducing the inhomogeneity of magnetic parameters, such as the local coercivity variation[9,10,21] or the local anisotropy variation.[22] All these efforts have enhanced our understanding of magnetization-reversal dynamics. However, the scope of those studies has been limited to small sample areas, due to the involved time-consuming iterative algorithms. A fast characterization algorithm of the reversal behavior is thus challenging in the most practical analysis. As an explicit approach, Choe *et al.*[24] recently proposed an analytic description of the magnetization-reversal phase diagram, which basically involves three different phases with respect to the magnetostatic energy and the domain-wall energy. In this work, we have fully investigated the characteristics of magnetization reversal in perpendicular anisotropy films by extending this approach to dependence on the observation size, the applied field strength, the temperature, and the magnetic anisotropy, as well as considering the local magnetic inhomogeneity and the relevance of nucleation sites.

II. DESCRIPTION OF THE THEORY

A micromagnetic model of uniaxial perpendicular anisotropy film, originally proposed by Kirby *et al.*,[17] has been adopted for this study. Briefly, the model describes a film consisting of nanosized identical single-domain cells on two-dimensional hexagonal lattices with a periodic boundary condition. Each cell has its magnetization aligned perpendicularly to the film plane. Magnetic domain walls form at the boundary between cells having opposite magnetization. We ignore the details of the wall configuration, but consider only the value of the wall energy density. The energy barrier of the switching process is then explicitly given by a function of magnetic and geometric parameters, i.e., of the saturation magnetization M_s, the uniaxial perpendicular magnetic anisotropy K_u, the domain-wall energy density σ_w, the cell volume V_c, and the film thickness t_f. Based on such an energy-barrier scheme, the switching of the magnetization in a cell is determined by a Monte Carlo algorithm. By iterating the reversal determination of the cells and mapping them onto a two-dimensional lattice, we construct the domain evolution patterns with time. Simulation results have shown that there exist three peculiar domain states formed by the typical reversal processes: (1) large domains via the wall-motion process, (2) dendritelike stripe domains via the dendritic-

TABLE I. Values of the parameters controlling the magnetization-reversal processes. Here, $\hat{h}_{stripe}$ is the contribution to the demagnetizing energy from the cells lying on the linear stripe domain and $\hat{h}_{self}$ is the self-demagnetizing energy of a cell. N is the total number of the simulation cells.

	$\hat{h}$	ζ	n
Wall motion	0	0	$N^{1/2}$
Stripe growth	$-1+\hat{h}_{stripe}$	2/3	2
Nucleation	$-1+\hat{h}_{self}$	1	N

growth process, and (3) randomly distributed small nucleated domains via the nucleation process.[18,24]

To characterize these contrasting domain patterns, we propose an analytic description of the magnetization phase diagram. Details of the model were described previously.[24] In this model we consider the three reversal processes mentioned above. Each reversal process is characterized by specific values of the following parameters: the domain wall coverage ζ, the normalized demagnetizing field $\hat{h}$, and the number of cells n. The values are listed in Table I. The domain-wall coverage ζ corresponds to the fractional ratio of new-forming wall length. It has a maximum of 1 for a nucleation situation, while it has a value of about 0 for a wall-motion process. The normalized demagnetizing field $\hat{h}$ is the ratio of the demagnetizing field to its saturation value. The demagnetizing field has a maximum for the nucleation case, while it is negligible for the wall-motion case due to the presence of almost equal areas of up- and down-surrounding domains. The reversal process of each cell is determined by the surrounding reversal situation: most unreversed cells have the nucleation situation, while the cells at the domain boundary can be reversed by wall motion, or a few cells at the end of stripes can be grown by stripe growth. The number of cells n for each process is determined in this manner.

The total probability P_i of a typical reversal situation i is taken into account. The total reversal probability P_i is equal to the sum of the probabilities of individual cells for a reversal situation i. The phase boundary between the i and j processes is then obtained by considering the balance between the total probabilities of the reversal processes, i.e.,

$$P_i = P_j. \tag{1}$$

We rewrite the total reversal probability as

$$P_i = \sum_{n_i} p_i \sim n_i p_i, \tag{2}$$

where p_i is the individual reversal probability of a cell and n_i is the number of cells for a reversal process i. In general, the wall-motion process has a larger individual reversal probability p than that of the nucleation process, but it has a smaller number of cells n than the other. Thus, in many cases the total reversal probability P is comparable between these processes. Equation (1) is then rewritten as in Ref. 24:

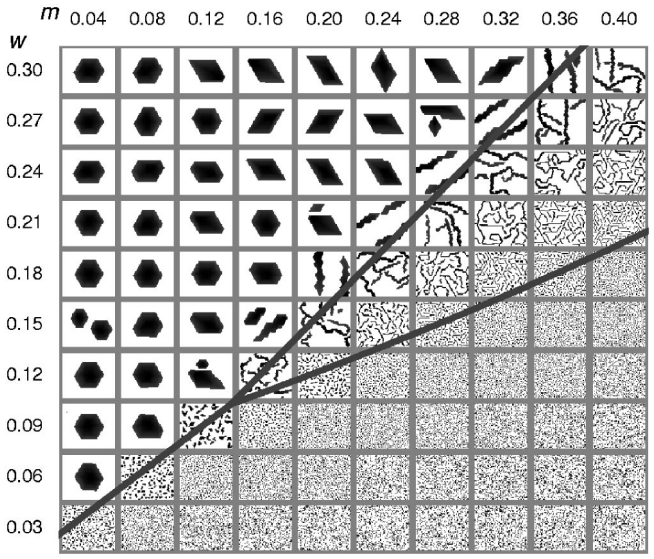

FIG. 1. Simulated domain patterns at 25% reversal with respect to the magnetostatic energy m (top scale) and the domain-wall energy w (left scale). Each frame is aligned in column with m and in row with w. α and β' values are given in the text. Phase equilibrium lines determined by Eq. (3) are shown in gray.

$$\beta'[2(1+\alpha)+m(\hat{h}_i+\hat{h}_j)+w(\zeta_i+\zeta_j)][m(\hat{h}_i-\hat{h}_j)+w(\zeta_i-\zeta_j)] = \log(n_i/n_j). \tag{3}$$

Four dimensionless parameters are introduced:

$$m = 2\pi M_s^2/K_u,$$

$$w = \sigma_w/t_c K_u,$$

$$\alpha = M_s H/2K_u,$$

$$\beta' = K_u V_c/k_B T, \tag{4}$$

where m, w, and α are the ratios of the magnetostatic energy, the wall energy, and the Zeeman energy to the anisotropy energy, respectively. β' is the thermal stability parameter, i.e., the ratio of the magnetic anisotropy energy of a cell over the thermal activation energy $k_B T$. t_c is the distance between the centers of the nearest-neighboring cells and roughly corresponds to the diameter of the grains or the activation volume. Using the reversal parameters listed in Table I, one can obtain the phase equilibrium relations between magnetic parameters.

III. RESULTS AND DISCUSSION

A. Phase diagram in uniform films

Figure 1 illustrates the simulated domain evolution patterns of ferromagnetic thin films with respect to the magnetostatic energy and the domain-wall energy using a 128 $\times$128 cell lattice. Each frame shows the domain evolution pattern of 25% reversal for a sample with magnetostatic energy and the domain-wall energy values denoted in the top

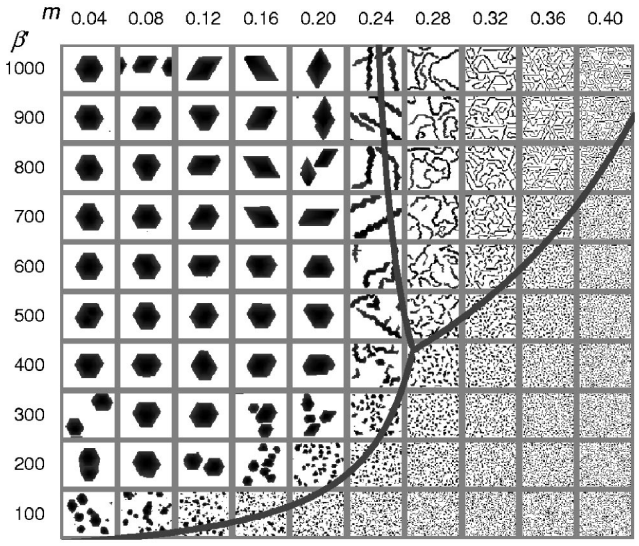

FIG. 2. Simulated domain patterns at 25% reversal with respect to the magnetostatic energy m (top scale) and the thermal stability parameter β' (left scale). Each frame is aligned in column with m and in row with β'. α and w values are given in the text. Phase equilibrium lines are shown in gray.

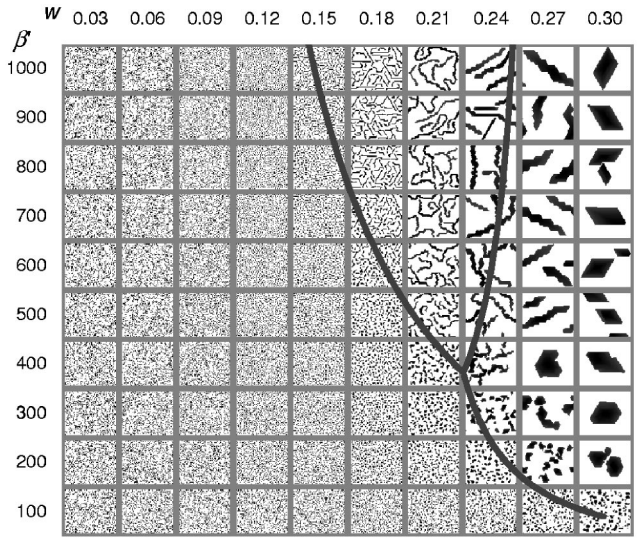

FIG. 3. Simulated domain patterns at 25% reversal with respect to the domain-wall energy w (top scale) and the thermal stability parameter β' (left scale). Each frame is aligned in column with w and in row with β'. α and m values are given in the text. Phase equilibrium lines are shown in gray.

and left sides, respectively. Here, the two other parameters, $\beta'=837$ and $\alpha=-0.75$, are fixed. The value of β' corresponds to $K_u=5\times10^5$ J/m^3, $t_c=t_f=50$ nm, and $T=300$ K. The figure shows three different magnetization reversal states: a large domain, dendritelike stripe domains, and randomly distributed small domains. All these patterns systematically change with the magnetic parameters, and the transition is shown between the reversal phases. The fundamental shape of the reversal patterns is unchanged with respect to the elapsed time and thus, it is considered as an invariant feature. The phase equilibrium lines are defined from Eq. (3) and plotted as the gray lines on the figure.

The transition between the wall motion and the nucleation dominant reversal is easily understood, since a larger wall energy prefers larger domains, whereas a larger magnetization prefers smaller domains as a ground energy state of domain patterns. The dendritic-growth process also relates to the ground energy state of the domain patterns. The dynamics of magnetization reversal is a relaxation process to the lowest (or ground) energy state for a given external magnetic field. The ground energy state of ultrathin magnetic films has been extensively studied, and a number of films showed mazelike domains, of which the stripe width is determined by the magnetic parameters.[25–27] The dendritic growth is thus the process approaching mazelike stripe domain patterns, when the film has the ground energy state of these patterns. In the simulation, the different reversal parameters induce the different energy barriers, which are known to be essential for the dendritic-growth process.[18]

Similar phase diagrams were deduced either in the m-β' or w-β' space, as shown in the Figs. 2 and 3, respectively. Here, we fixed the other parameters as $w=0.2$ in Fig. 2 and $m=0.3$ in Fig. 3. The α was kept as -0.75 for both the cases. These phase diagrams predict the phase transitions with respect to the temperature. With increasing temperature, the magnetization-reversal phase changes from either wall-motion or dendritic-growth dominant reversal to a nucleation dominant reversal. This comes from the different temperature dependence of the reversal probabilities. For an extreme case of high temperature, all the individual reversal probabilities p of each cell approach one and the total probability P is then solely determined by the number of cells n for each reversal process. Hence, the nucleation process having the largest number of the cells becomes dominant at high temperature. On the other hand, the dendritic-growth dominant reversal phase corresponding to the smallest number of cells, can be observed only when the experiment is carried out at a sufficiently low temperature, or if the sample has a sufficiently large anisotropy and cell volume. We exclude the temperature dependence of the other parameters here, but one can easily include it if it is given for a specific film system.

Since the thermal stability parameter β' also depends on the cell volume used in the simulations, the cell volume must be carefully chosen by consideration of the sample properties. We believe that it is most reasonable to make the cell volume equal to either the activation volume or the grain size. The activation volume V_a has been reported to be in the range of 3.0×10^{-24} m$^3<V_a<1.9\times10^{-23}$ m^3 for Co/Pd multilayer films,[28] 1.6×10^{-23} m$^3<V_a<6.8\times10^{-23}$ m^3 for TbCoGd and GdFe alloy films,[13] and 1.0×10^{-25} m$^3<V_a<2.9\times10^{-24}$ m^3 for Au/Co/Au films.[29,30]

It is worthwhile to compare the present phase diagram with experimental observations. The transition between the wall-motion and the dendritic-growth dominant phases among Co/Pd multilayer films was explained by the change in the saturation magnetization dependent on the Co-sublayer thickness.[15] This transition is seen in Fig. 1, with changing the saturation magnetization m from 0.05 to 0.20 on the row having the wall energy w of about 0.15. The other transition

was reported in Dy/Fe multilayer films.[17] The transition from the nucleation to the wall-motion dominant phase was observed with changing the wall energy, as seen in Fig. 1 on the column of $m=0.04$ with changing w from 0.03 to 0.09. This rough comparison well explains the reversal phases with respect to the magnetic parameters, but a quantitative comparison can be made if one knows the other parameters such as the strength of the applied magnetic field, the experimental temperature, and the grain or activation volume.

A fundamental question is whether the magnetization reversal exhibits an abrupt or a continuous phase transition with respect to the magnetic parameters. To answer this question, we have examined the reversal around the phase transition. The results revealed that all the transitions occurred by continuous changes in domain patterns. For instance, the transition between the wall-motion and nucleation dominant phases with changing domain wall energy exhibits a gradual increment in the average size of the domains together with a gradual decrease of the number of domains. Another continuous transition was observed between large domains and mazelike stripe domains with respect to the magnetostatic energy. As mentioned above, this smooth transition relates to the ground energy domain state, which shows a gradual change of the stripe width with changing magnetic parameters.[25,26] Note that even though the stripe width is sensitive to the magnetic parameters around the transition point, the change is continuous up to about a few microns.[27]

From the phase-transition equation, it is expected that the strength of an applied field also induces the phase change. However, in usual experimental conditions the effect is relatively small compared to that of the magnetostatic or domain-wall energy. Thus, generally an applied field does not result in any significant change, but a sample inherently exhibiting an intermediate reversal behavior can show a noticeable change with respect to the magnitude of an applied field. For an example we plot the reversal probability by nucleation and dendritic-growth process together with the simulated domain evolution patterns for a sample having magnetic properties close to the phase equilibrium condition in Fig. 4. The figure shows the phase transition from the nucleation dominant phase to the dendritic-growth dominant phase with increasing an applied field strength.

It is interesting to note that the reversal phase also changes with respect to the size of the simulation area. It is because the number of cells for the reversal processes has different dependence on the simulation area. The number of cells for the nucleation process increases proportionally to the total number of the simulation cells, while the number of cells for the other processes is restricted by existing domains. The nucleation process thus becomes more dominant with increasing the simulation size. We demonstrate the effect of the simulation size in Fig. 5. The domain evolution pattern in Fig. 5(a) seems to be a wall-motion dominant phase. But, if the domain evolution pattern is a part of a large area and the same patterns are repeated over the whole area of the sample, then the overall image becomes a nucleation dominant phase with lots of nucleation sites as seen in Fig. 5(c). To avoid any misleading result caused by the simulation size, it is important to confirm that the simulation is performed on the same area.

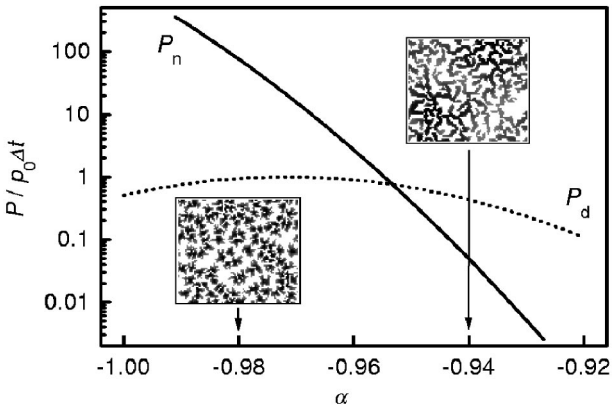

FIG. 4. Variation of nucleation probability P_n and the dendritic-growth probability P_d with respect to the strength of the reduced applied field value α. Magnetic parameters are taken as $m=0.5$ and $w=0.4$. Two simulated domain patterns are shown for the α values.

B. Effect of magnetic inhomogeneity

Local magnetic inhomogeneity possibly caused by structural imperfections was examined as another origin of the contrasting reversal behavior. To introduce the local magnetic irregularity, a random fluctuation is assigned to the magnetic anisotropy of each cell, since the anisotropy, rather than the magnetization, is sensitive to the structural irregularity in ferromagnetic thin films.[31] In our model, the anisotropy distribution $K_u(x,y)$ was chosen to be spatially noncorrelated and to have a Gaussian distribution in magnitude with the standard deviation δ,

$$K_u(x,y) = K_u^0[1 + \delta f(x,y)], \tag{5}$$

where K_u^0 is the mean value of the anisotropy and $f(x,y)$ is the spatially noncorrelated fluctuating function having a unit standard deviation. The same function $f(x,y)$ and the same magnetic parameters were used in the simulation, but the magnitude of the fluctuations δ was varied. Interestingly, the magnetization-reversal behavior was found to be very sensitive to the degree of anisotropy fluctuation. A large domain is formed in uniform films by an isotropic wall-motion process. But, the domains become ragged and finally split apart into

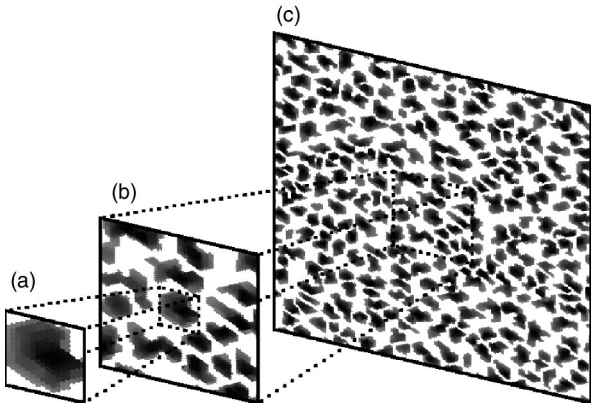

FIG. 5. Simulation size effect: (a) 16×16 cells in part of (b), (b) 64×64 cells in part of (c), and (c) 256×256 cells.

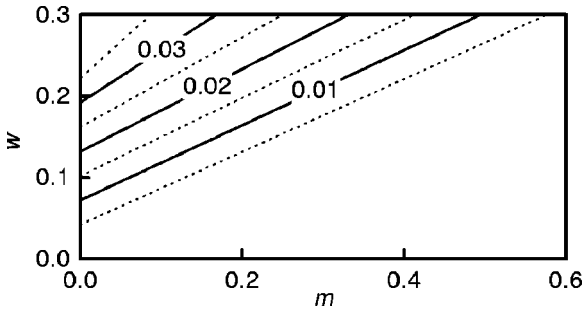

FIG. 6. Degree of the local magnetic variation for inducing a transition from a wall-motion or dendritic-growth dominant state to a nucleation dominant state in the (m,w) space.

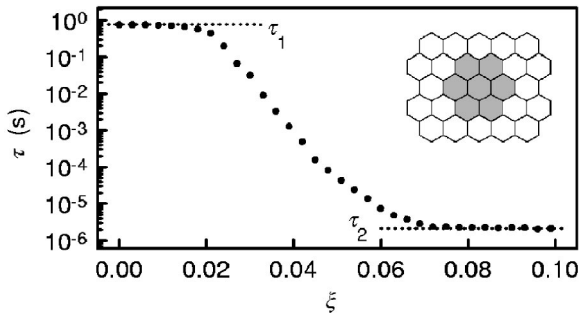

FIG. 7. The half-reversal time with respect to the anisotropy reduction rate ξ of the nucleation site. The dotted lines indicate the two distinct short and long time limits, τ_1 and τ_2. The inset shows the shape of the nucleation site composed of seven cells.

many small pieces with increasing anisotropy fluctuation. The average size of the small domains gradually decreases with increasing the local anisotropy variation. The wall-pinning effect due to local structural irregularities is introduced to explain this transition: a number of small domains having ragged domain boundaries appear when the wall-pinning effect is dominant, whereas a regular large domain is expected in uniform films. These ragged domains due to the local irregularities were observed in Co/Pt multilayer films[32] and Au/Co/Au films,[9] and theoretically explained by introducing the local distribution of the coercivity[9,21] to explain the magnetization process and the coercivity mechanism.

Here, we estimate how large the magnetic variation needs to be to induce a phase transition in terms of the local anisotropy variation. Considering the above local anisotropy variation given by Eq. (5), the energy barrier E_b is rewritten as

$$E_b = \frac{K_u^0 V_c}{1+\delta f}[1+\delta f + \hat{m}(\alpha + m\hat{h} + \zeta w)]^2. \tag{6}$$

In this case, the contrasting magnetization-reversal behavior is determined by the counterbalance between the values of δf and $m\hat{h}+\zeta w$, where the former term relates to the local anisotropy variation and the latter terms relate to the macroscopic magnetic parameters. A random scattered nucleation becomes dominant when the local anisotropy variation overcomes the other values. The degree of the local variation δf for a phase transition is thus proportional to the difference of $m\hat{h}+\zeta w$ between the processes. The simulation results are shown in the m-w coordinate space in Fig. 6. The local variation plays a more important role in a sample having a larger m and a smaller w, and a few percent of local anisotropy variation induces the phase transition to a random nucleation dominant phase.

Since the domain evolution always starts from nucleation sites, it is worthwhile to examine how a nucleation site affects the magnetization reversal dynamics. The simulation result revealed that the half-reversal time is very sensitive to the magnetic properties of a nucleation site, whereas the domain evolution pattern remains essentially the same. In this study, a nucleation site was assumed to be composed of seven cells having a smaller perpendicular magnetic anisotropy $K_u^{\mathrm{nuc}}=(1-\xi)K_u^0$ than most of surrounding cells having a mean perpendicular magnetic anisotropy K_u^0, where ξ is the reduction rate of the magnetic anisotropy ranging from 0 to 1. In Fig. 7, we plot the half-reversal time with respect to ξ. There exist two distinct bounds for the half-reversal time, τ_1 and τ_2, as guided by the dotted lines. τ_1 relates to the initial nucleation process being far slower than the wall-motion process. In the other limit, the initial nucleation is much faster than the wall propagation and thus, τ_2 is determined by the wall-motion process. The coercivity is also determined either by the nucleation or by the wall-motion process, depending on the properties of the nucleation sites. The shape of the magnetization viscosity curves is also sensitive to ξ. Figure 8 shows the typical magnetization viscosity curves for samples with ξ equal to (a) 0.00, (b) 0.07, and (c) 0.09, respectively. The abrupt decay shown in Fig. 8(a) is caused by the slow initial nucleation process and the fast wall-motion process, while the parabolic relaxation in Fig. 8(c) is due to the slow wall-motion process with a fast initial nucleation. These viscosity curves have been analyzed within the context of the Fatuzzo's phenomenological model,[13,33] and all curves in the figure are known as the particular shape of the wall-motion dominant reversal. Even though all the samples show the same wall-motion dominant reversal, the property of the nucleation site plays a role in determining the shape of the viscosity curve.

IV. CONCLUSIONS

The stability of reversed magnetic domain states in ferromagnetic thin films with perpendicular magnetic anisotropy

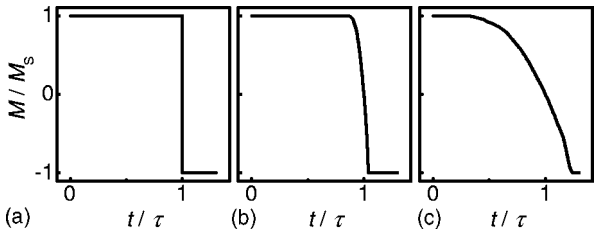

FIG. 8. The typical magnetization viscosity curves for samples with ξ equal to (a) 0.00, (b) 0.07, and (c) 0.09, respectively. The x axis is the time t normalized by the half magnetization-reversal time τ and the y -axis is the magnetization M normalized by the saturation magnetization M_s. All samples have the same magnetic parameters of $m=0.7$ and $w=0.2$.

has been investigated by Monte Carlo micromagnetic simulations. The evolution of the simulated domain patterns with geometric and magnetic parameters can be classified into three contrasting magnetization reversal phases: (i) wall motion, (ii) dendritic growth, and (iii) nucleation state. We deduced the phase diagram for the three reversal states and determined the phase equilibrium lines. The phase diagram provides useful predictions on reversed states without carrying out time-consuming simulations. The reversal state is mainly determined by the magnetostatic energy, the domain-wall energy, the temperature, and the local magnetic variations. However, it also depends on the anisotropy, the cell volume, the applied field, and the simulation size. All phase transitions proceeded by gradual changes between the contrasting reversal phases. The local magnetic irregularity also induces a phase transition with a few percent change of the anisotropy variation. The shapes of the viscosity curves contrastingly change with respect to the properties of the nucleation site even for the same domain evolution mechanisms.

ACKNOWLEDGMENT

This work was supported by the Korean Ministry of Science and Technology through the Creative Research Initiatives Project.

[1] J. L. Simonds, Phys. Today **48** (4), 26 (1995).
[2] K. M. Krishnan, MRS Bull. **20** (10), 24 (1995).
[3] G. A. Prinz, Science **282**, 1660 (1998).
[4] H.-P. D. Shieh and M. H. Kryder, J. Appl. Phys. **61**, 1108 (1987).
[5] S.-B. Choe, D.-H. Kim, Y.-C. Cho, H.-J. Jang, K.-S. Ryu, H.-S. Lee, and S.-C. Shin, Rev. Sci. Instrum. **73**, 2910 (2002).
[6] J. X. Shen, R. D. Kirby, Z. S. Shan, D. J. Sellmyer, and T. Suzuki, J. Appl. Phys. **73**, 6418 (1993).
[7] J. Pommier, P. Meyer, G. Pénissard, J. Ferré, P. Bruno, and D. Renard, Phys. Rev. Lett. **65**, 2054 (1990).
[8] H.-P. D. Shieh and M. H. Kryder, IEEE Trans. Magn. **24**, 2464 (1988).
[9] J. Ferré, V. Grolier, P. Meyer, S. Lemerle, A. Maziewski, E. Stefanowicz, S. V. Tarasenko, V. V. Tarasenko, M. Kisielewski, and D. Renard, Phys. Rev. B **55**, 15092 (1997).
[10] I. J. Ferré, *Spin Dynamics in Confined Magnetic Structure* (Springer-Verlag, Berlin, 2002), p. 127; B. D. Cullity, *Introduction to Magnetic Materials* (Addison-Wesley, Reading, MA, 1972), Chap. 2, Sec. 6.
[11] S.-B. Choe and S.-C. Shin, Phys. Rev. B **62**, 8646 (2000).
[12] C.-J. Lin, J. C. Suit, and R. H. Geiss, J. Appl. Phys. **63**, 3835 (1988).
[13] M. Labrune, S. Andrieu, F. Rio, and P. Bernstein, J. Magn. Magn. Mater. **80**, 211 (1989).
[14] R. D. Kirby, J. X. Shen, Z. S. Shan, and D. J. Sellmyer, J. Appl. Phys. **70**, 6200 (1991).
[15] S.-B. Choe and S.-C. Shin, Phys. Rev. B **57**, 1085 (1998).
[16] T. G. Pokhil and N. Nikolaev, IEEE Trans. Magn. **29**, 2536 (1993).
[17] R. D. Kirby, J. X. Shen, R. J. Hardy, and D. J. Sellmyer, Phys. Rev. B **49**, 10810 (1994).
[18] A. Lyberatos, J. Earl, and R. W. Chantrell, Phys. Rev. B **53**, 5493 (1996).
[19] A. Lyberatos, J. Phys. D **33**, R117 (2000).
[20] U. Nowak, J. Heimel, T. Kleinefeld, and D. Weller, Phys. Rev. B **56**, 8143 (1997).
[21] A. Lyberatos, J. Magn. Magn. Mater. **186**, 248 (1998).
[22] S.-B. Choe and S.-C. Shin, IEEE Trans. Magn. **36**, 3167 (2000).
[23] M. Mansuripur, J. Appl. Phys. **61**, 1580 (1987).
[24] S.-B. Choe and S.-C. Shin, Appl. Phys. Lett. **80**, 1791 (2002).
[25] H. J. G. Draaisma and W. J. M. de Jonge, J. Appl. Phys. **62**, 3318 (1987).
[26] Y. Yafet and E. M. Gyorgy, Phys. Rev. B **38**, 9145 (1988).
[27] S.-B. Choe and S.-C. Shin, Phys. Rev. B **59**, 142 (1999).
[28] S.-B. Choe and S.-C. Shin, Phys. Rev. Lett. **86**, 532 (2001).
[29] A. Kirilyuk, J. Ferré, J. Pommier, and D. Renard, J. Magn. Magn. Mater. **121**, 536 (1993).
[30] B. Raquet, R. Mamy, and J. C. Ousset, Phys. Rev. B **54**, 4128 (1996).
[31] H. Kronmüller, Phys. Status Solidi B **144**, 385 (1987).
[32] B. E. Bernacki and M. Mansuripur, J. Appl. Phys. **69**, 4960 (1991).
[33] E. Fatuzzo, Phys. Rev. **127**, 1999 (1962).